Development of model-based fault diagnosis algorithms for MASCOTTE cryogenic test bench

A. Iannetti[1,3], **J. Marzat**[2], **H. Piet-Lahanier**[2], **G. Ordonneau**[2] , **L. Vingert**[2]
E-mail: alessandra.iannetti@cnes.fr

Abstract. This article describes the on-going results of a fault diagnosis benchmark for a cryogenic rocket engine demonstrator. The benchmark consists in the use of classical model-based fault diagnosis methods to monitor the status of the cooling circuit of the MASCOTTE cryogenic bench. The algorithms developed are validated on real data from the last 2014 firing campaign (ATAC campaign). The objective of this demonstration is to find practical diagnosis alternatives to classical redline providing more flexible means of data exploitation in real time and for post processing.

1 Introduction

Model-based fault detection methods are one of the most common diagnostic technics used in process monitoring for a wide range of applications (ex. nuclear, aeronautics, chemical etc.) [1], [2],[3]. A mathematical model represents the knowledge of the process and it is used to produce diagnosis flags based on deviations of parameters from their nominal expected values. These deviations (residuals) can be obtained from the evaluation of characteristic parameters of the system as in parameter estimation methods [4] or directly from sensor output estimation as in Kalman filtering approaches [5]. Finally statistical tests on the residuals are performed to obtain robust diagnosis flags (i.e. CUSUM test [6], [14]).

In the field of rocket engines, fault detection and diagnosis technics are called health monitoring systems (or health management systems if reconfiguration actions are possible). So far rocket engine diagnosis has been performed mostly via simple redlines over preselected sensors (fixed threshold). This approach has been preferred as it is simple and requires low computation effort. On the other hand its drawbacks are the high number of sensors and thresholds to be set for each targeted engine operating point leading to higher possibility of human errors and unjustified firing aborts. During the last decades, an important number of researches [7] have been dedicated to the improvement of the diagnosis methods for applications at test bench or during flight [8][9][10][11]. The difficulty of these systems is the complexity of the processes to monitor and the need for reliable diagnosis with short reaction times (from 10 milliseconds up to a few seconds).

The aim of this work is to find new possible alternatives to simple redline checking for the cryogenic rocket engine demonstrator MASCOTTE. Two diagnosis methods have been developed here, namely parameter identification and Kalman filtering. These methods have been implemented and tested on real data from the latest firing campaign of 2014 for the bi-dimensional nozzle ATAC [12].

[1] CNES launchers directorate, 52 rue Jacques Hillairet, 75012 Paris, France
[2] ONERA - The French Aerospace Lab, F-91123 Palaiseau, France
[3] Author to whom any correspondence should be addressed

2 Mascotte description

MASCOTTE test bench was designed to study cryogenic rocket combustion and nozzle flow performances. It was built in 1994 from the cooperation of CNES and ONERA. Several version of the hardware were developed during the years for different purposes. The most recent version called ATAC is used to analyse rocket nozzle performances. The combustion chamber fed with gaseous hydrogen and oxygen is terminated by a 2D nozzle. The hardware has been equipped with a water cooling circuit in order to withstand high mixture ratio and pressure in the chamber and to operate for longer duration (around 60s). Figure 1 shows the chamber section and the bi-dimensional nozzle [12].

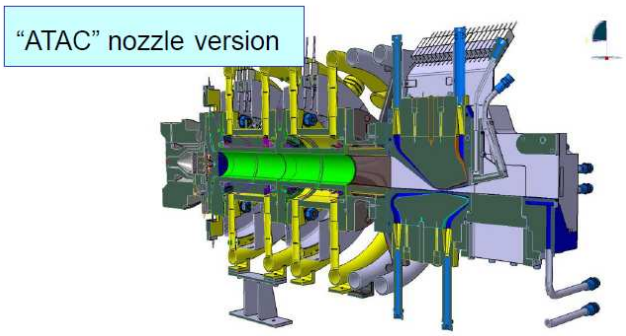

Figure 1 Combustion and nozzle section with water cooling system (yellow circuit for the chamber part and blue circuit for the nozzle part)

The bench is monitored and controlled via three main computers. The initial diagnosis system is based on independent redlines on relevant parameters. In particular for the water circuit all pressures, temperatures and mass flows are monitored and a test stop is issued whenever one or more of these parameters cross a redline for more than a minimum time. The redlines are set manually by the experts and validated via a dedicated bench firing before each test campaign. The bench is in open-loop control and only test abort over redlines or nominal test stop are possible. Figure 2 shows the water circuit architecture of the bench.

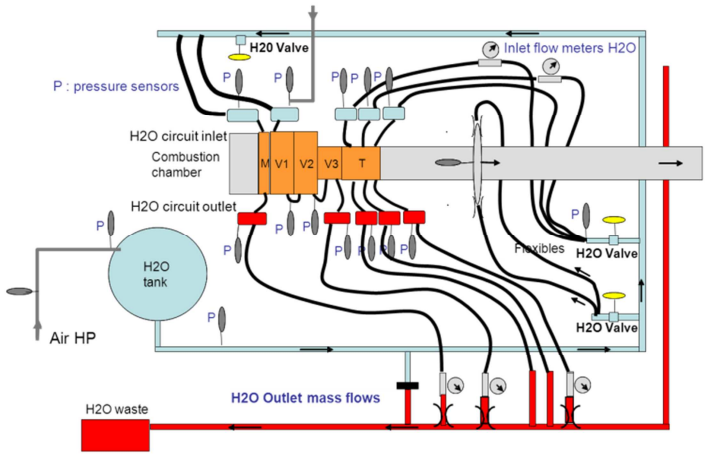

Figure 2 Test bench water cooling circuit: M = inlet chamber section, V1 to V3 = middle chamber sections, T = nozzle.

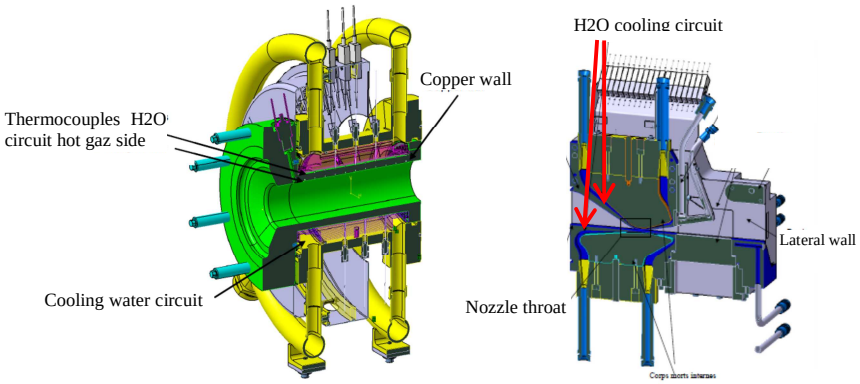

Figure 3 Chamber and nozzle section: water cooling detail.

3 Fault diagnosis methods

The selected methods for the diagnosis demonstration are classical model-based technics [1], [3]:

- Least-square parameter identification
- Kalman filter

An analysis of the possible modelling of the cooling system was performed and a simplified model was set up for describing the main processes in each branch of the water circuit. This model is the basis of the diagnosis strategy.

4 Water cooling system model

The chamber or nozzle section in Figure 3 is modelled through an inlet cavity, an orifice and an outlet cavity. Figure 4 shows the corresponding zones. Cavity 1 corresponds to the inlet volume of the cooling circuit, the orifice is the connecting tube and cavity 2 the water volume flowing on the chamber wall and heated up by the combustion process. This scheme can be applied to any other segment of the water circuit: the three chamber segments (V1 and V2, V3 in Figure 2) and the bi-dimensional nozzle part (T in figure 2). The only difference is in the parameter of the model depending on the geometry.

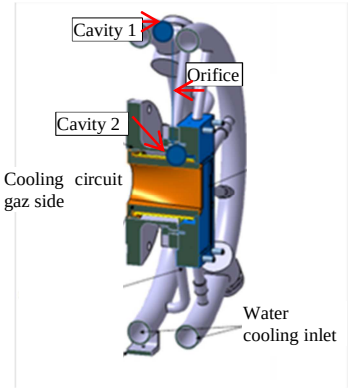

Figure 4 Water cooling modelling

This modelling approach is directly derived by the CNES software CARMEN [18] which is used for rocket engine systems modelling. It was extensively validated on different engines and propulsive systems. The idea here is to build a simple and generic model, but representative of the system dynamics and generic enough to be applicable to different system parts. The governing equations obtained from conservation laws applied to each element are given in equations (1), (2) and (3).

Cavity 1:

$$\frac{dP_1}{dt} = (q_1^e - q_1^s) \cdot \frac{a^2}{V_1}$$
$$\frac{dT_1}{dt} = \frac{1}{\rho \cdot V_1} \cdot (q_1^e T_1^e - q_1^s T_1) + \frac{\dot{Q}_1}{c_v \rho V_1} \quad (1)$$

Liquid orifice:

$$P_1 - P_2 = \frac{k_p}{\rho S^2} \cdot q^2$$
$$q = \sqrt{\frac{P_1 - P_2}{k_p} \cdot \rho S^2} \quad (2)$$

Cavity 2:

$$\frac{dP_2}{dt} = (q_2^e - q_2^s) \cdot \frac{a^2}{V_2}$$
$$\frac{dT_2}{dt} = \frac{1}{\rho \cdot V_2} \cdot \left(q_2^e T_2^e - q_2^s T_2\right) + \frac{\dot{Q}_2}{c_v \rho V_2} \quad (3)$$

List of variables:

P_1: pressure in cavity 1 (Pa)
P_2: pressure in cavity 2 (Pa)
k_p : pressure drop coefficient (non dimensional)
ρ : water density (kg/m^3)
a : speed of sound in water (m/s)
c_v: specific heat of water at constant volume
V_1 : volume of cavity 1 (m^3)
V_2 : volume of cavity 2 (m^3)
S : cross sectional area for the orifice element (m^2)
$q = q_1^s = q_2^e$: mass flow through the orifice element / outlet mass flow from cavity 1/ inlet mass flow to cavity 2 (kg/s)
q_1^e : cavity 1 inlet mass flow (kg/s)
q_2^s : cavity 2 outlet mass flow (kg/s)
T_1 : temperature in cavity 1 (K)
T_2 : temperature in cavity 2 (K)
$\dot{Q}_1$: heat flux on cavity 1 (W)
$\dot{Q}_2$: heat flux on cavity 2 (W)

Let consider first equations (1), (2) for establishing a model of pressure and mass flow evolution. Assuming $q_1^s = q_2^e$ the resulting equation, for each branch of the circuit is equation (4) below.

$$\frac{dP_2}{dt} = \left(\sqrt{\frac{P_1 - P_2}{k_p} \cdot \rho S^2} - q_2^s\right) \cdot \frac{a^2}{V_2} \quad (4)$$

4.1 Pressure drop coefficient

The pressure drop coefficient, k_p is calculated via a Blasius correlation [13] applicable for Reynolds number higher than 5000. This was verified on past nominal firing campaign as shown in Figure 5.

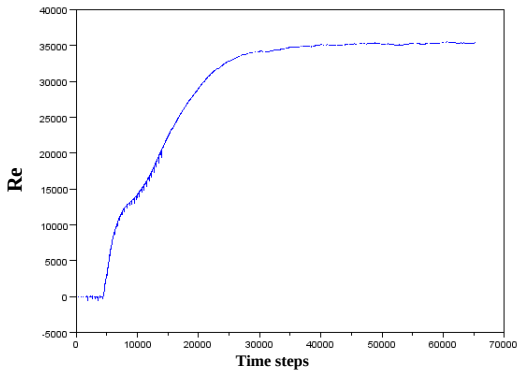

Figure 5 Reynolds number in water cooling chamber branch for a nominal Mascotte firing campaign (time in milliseconds)

The correlation is expressed in equation (5).

$$P_1 - P_2 = \Lambda \cdot \frac{L}{D_h} \cdot \frac{\rho \cdot v^2}{2}$$
$$\Lambda = 0.3164\, Re^{-0.25} \quad (5)$$

With:

$Re = \frac{D_h \cdot v \cdot \rho}{\mu}$ Reynold number (non-dimensional)
v = average speed in flow cross section (m/s)
μ = dynamic viscosity (kg/(s m))
D_h= characteristic dimension cross flow, hydraulic diameter
L = characteristic length of the flow

Rewriting the expression above with the mass flow rate expression $q = \rho \cdot v \cdot S$, we obtain:

$$K = 0.3164 \cdot \left(\frac{Q}{\frac{\pi D}{4} \cdot \mu} \right)^{-0.25} \cdot \frac{L}{D} \cdot \frac{1}{2} \quad (6)$$

Introducing the parameter $M = 0.3164 \cdot \left(\frac{1}{\frac{\pi D_h}{4} \cdot \mu} \right)^{-0.25} \cdot \frac{L}{D_h} \cdot \frac{1}{2}$ and the derivative of state variable $\dot{P}_2 = \frac{dP_2}{dt}$ in equation (4), we obtain equation (7).

$$\dot{P}_2 = \frac{a^2}{V_2} \cdot \left(-q_2\,(t) + q_2^{0.125}(t) \cdot \sqrt{\frac{\rho \cdot S^2}{M}} \cdot \sqrt{P_1(t) - P_2(t)} \right) \quad (7)$$

It should be noted that this model is only valid when P1>P2, otherwise, a flag could be raised.

4.2 Final water cooling system model

With additional constant parameters $b = \frac{a^2}{V}$, $c = \left(\frac{\rho \cdot S^2}{M} \right)^{\frac{1}{2}}$, the final model is expressed in equation (8).

$$\dot{P}_2 = b \cdot \left(-q_2(t) + c \cdot q_2^{0.125}(t) \cdot \sqrt{P_1(t) - P_2(t)} \right) \quad (8)$$

This equation will be applied to the chamber or the nozzle sections of the water cooling circuit with a measured mass flow either at outlet or inlet.

5 Geometrical evaluation of equation parameters b, c and M

Geometrical data of each part of the water cooling circuit makes it possible to determine the numerical values for parameters c and b in equation (8). The obtained values are characteristic quantities of the given water circuit section supposed to be always constant.

The practical difficulty in their evaluation from their analytical expression is that the volumes of the cavities indicated in Section 4 cannot be precisely identified and depend also on the measurement location. The following evaluations constitute thus first guesses including measurement and modelling uncertainty: they will be verified on real data for nominal cases. For diagnosis purpose the reference value can also be identified through the method in Section 6.

Table 1. First evaluations of *b*, *c* and *M*

section	***b***	***c***	***M***
chamber	4.4 E-11	0.0045	0.12
nozzle	5E-11	0.0016	0.36

The above values are calculated with assumptions of constant values for the following physical data of water:

Table 2. Thermo physical data for water

Property	**value**	**unit**
Density, ρ	980	kg/m^3
Dynamic viscosity, μ	0.001	kg/m/s

6 Parameter identification algorithm

The model used in this section is derived from expression (8) with assumption of $\dot{P}_2 \sim 0$, and is thus applicable only in steady-state conditions.

$$q_2(t) = c \cdot q_2^{0.125}(t) \cdot \sqrt{P_1(t) - P_2(t)} \tag{9}$$

A recursive least-square identification algorithm is employed for estimating the value of *c* based on the measurements of q_2 , P_1 and P_2. Equation (9) can be written under the form $y = h \cdot c$ where $y = q_2(t)$ and $h = q_2^{0.125}(t) \cdot \sqrt{P_1(t) - P_2(t)}$.

The parameter is initialized with $c(0) = c_0$, where c_0 can be a geometrical guess from Section 5, and the parameter variance $v(0) = v_0$. The update at time step *k* is then performed as follows, to minimize $\|Y_N - H_N\|_2^2$ where Y_N and H_N are the sequences of *y* and *h* from time 0 to *N*.

$$\begin{aligned} \alpha(k) &= y(k) - h(k) \cdot c(k-1) \\ g(k) &= v(k-1)h(k)\big(\gamma + h(k) \cdot v(k-1) \cdot h(k)\big)^{-1} \\ c(k) &= c(k-1) + g(k) \cdot \alpha(k) \\ v(k) &= c(k-1) + g(k) \cdot \alpha(k) \end{aligned} \tag{10}$$

The parameter γ is an exponential forgetting factor: it allows giving more importance to recent data from sensors in the recursive scheme and accounting for unmodelled slow parameter variation. The residual considered can be the difference between *c(k)* and a known value c_{ref}, or the update residual $\alpha(k)$ [7]. Here, the first solution was retained (the second one is similar to the Kalman filter strategy developed in the next section).

7 Kalman filter fault diagnosis

The Kalman filter model allows to estimate at the same time the system characteristic parameters (just as seen with *b* and *c* in the model) and one or more state variables [5]. In the chosen example we decided to estimate the outlet (or inlet) pressure and the parameter $d = b \cdot c$. The inputs are the measured pressure and the mass flow (respectively inlet or outlet). There is no need to make assumptions on pressure derivatives to obtain the Kalman algorithm as needed to obtain equation (9)

for the parameter identification approach. The filter is also efficient during transient phases. The state-space model can be written in discrete time form with time step *k*. The Kalman prediction is given in equation (11).

$$X(k+1) = f_d(U(k), X(k)) = X(k) + dt \cdot f(X(k), U(k)) \tag{11}$$

The input vector is $U = [q_2, P1]$ and the state variables vector is $X = [P2, d]$. The expression of $f(X(k), U(k))$ with $d = b \cdot c$ obtained from equation (8) is given in equation (12).

$$\begin{aligned} \dot{P}_2 &= -bq_2\,(t) + d \cdot q_2^{0.125}(t) \cdot \sqrt{P_1(t) - P_2(t)} \\ \dot{d} &= 0 \end{aligned} \tag{12}$$

Since this state-space model is nonlinear, an Extended Kalman filter (EKF) is considered (other extensions of Kalman filter, such as UKF, will be considered for future versions). The derivatives for equation (11) are $F_k = \frac{\partial f_d}{\partial X}\Big|_{X=X_k}$ and $L_k = \frac{\partial f_d}{\partial U}\Big|_{U=U_k}$, and the coefficients in equations (13) can be obtained from equations (11) and (12).

$$\begin{aligned} F_k(1,1) &= 1 + dt \cdot \left(\frac{X(k-1,2)}{2} \cdot U(k,1)^{0.125} \left(\frac{1}{U(k,2) - X(k-1,1)} \right)^{\frac{1}{2}} \right) \\ F_k(1,2) &= -dt \cdot \left(U(k,1)^{0.125} \sqrt{U(k,2) - X(k-1,1)} \right) \\ F_k(2,1) &= 0 \\ F_k(2,2) &= 1 \\ L_k(1,1) &= dt \cdot \left(-b + X(k-1,2) * 0.125 * U(k,1)^{0.125} \cdot \sqrt{U(k,2) - X(k-1,1)} \right) \\ L_k(1,2) &= -dt \cdot \left(\frac{X(k-1,2)}{2} \cdot U(k,1)^{0.125} \cdot \left(\frac{1}{U(k,2) - X(k-1,1)} \right)^{\frac{1}{2}} \right) \\ L_k(2,1) &= 0 \\ L_k(2,2) &= 0 \end{aligned} \tag{13}$$

The covariance matrix is predicted with the above coefficients as in equation (14):

$$Cov_{k|k-1} = F_{k-1}\, Cov_{k-1|k-1}\, F_{k-1}^T + L_{k-1}\, Q_{k-1}\, L_{k-1}^T + M_{k-1} \tag{14}$$

Where *Q* is the covariance matrix of the input noise for *U* and is based on the sensor noise and M is the covariance matrix of the state noise. Introducing the value $\widehat{Y_k}$ as the residual between the Kalman prediction and measured values Z_k (here is P1 or P2, the parameter d is only estimated, not measured), the residual obtained is given in equation (15).

$$\widehat{Y_k} = Z_k - C_k \hat{X}_{k|k-1} \tag{15}$$

The variance of the residual is expressed in equation (16) in terms of the state covariance matrix Cov and the measurement covariance matrix R_k (pressure measurement noise).

$$S_k = C_k Cov_{k|k-1} C_k^T + R_k \tag{16}$$

The Kalman filter gain expression is given in equation (17).

$$K_k = Cov_{k|k-1} C_k^T S_k^{-1} \tag{17}$$

The Kalman filter is used to update the X_k estimate and the covariance matrix Cov as described in equation (18).

$$\begin{aligned} &\hat{X}_{k|k} = \hat{X}_{k|k-1} + K_k \widehat{Y_k}\,, \\ &Cov_{k|k} = (I - K_k C_k) Cov_{k|k-1} \end{aligned} \tag{18}$$

The residual Y_k can be taken before or after the Kalman correction depending on the balance between the reliability of the model and of the available measurements. For this demonstration the residual is taken after Kalman correction at the end of each calculation step.

8 Residual analysis for decision

The outputs provided by the diagnosis algorithms are residuals that can be processed to raise detection flags. For the parameter identification approach, the residual is the difference between the estimated parameter *c* and its reference identified value. This value is constant during steady-state nominal operations (less than 1% noise as verified in the various firing tests used for validation). For the Kalman filter approach the value of the residual Y_k is directly the difference between the estimated state variable and its measured value. The diagnosis parameters are thus analyzed via the CUSUM test expressed in equations (19) [6],[14],[15] .

$$S_1(t) = \max(S_1(t-1) + r(t) - \mu_0 - \delta/2, 0)$$
$$S_2(t) = \max(S_2(t-1) - r(t) + \mu_0 - \delta/2, 0) \quad (19)$$

The parameter δ is the minimal size of the faulty variation to be detected. The decision rule is then expressed in equations (20).

if ($S_1 > \lambda$) or ($S_2 > \lambda$) ⇒ decide fault
else ⇒ decide no fault
λ is a user threshold. (20)
r(t) is the residual
μ_0= residual average

The value of δ can be set to the maximum allowable variation of the diagnostic parameter or the minimum detectable change. The value of threshold λ is based on the allowable detection delay.

9 Validation on real data

The developed tools have been at first validated using data from different firing campaigns of 2010 and 2014. The estimated value of parameter *c* has been compared to those obtained from test data and the maximum difference observed is lower than 10%. This parameter is observed to remain constant during nominal steady state operation regardless of the pressure and mass flow conditions in the system. It thus constitutes a viable reference parameter for the residual calculation.
Kalman estimation error for the pressure component proved to be less than 1% error.
In this section, one firing test is selected to present an example of application on a faulty behaviour. The algorithms are applied on the chamber section (V2 in Figure 2) and on the nozzle (section T in Figure 2). The monitored sensors are inlet /outlet pressure and mass-flow (P1, P2, q2).

9.1 ATAC campaign, May 14th 2014 results

During this test the MASCOTTE bench was fired with the bi-dimensional nozzle configuration ATAC. The test was nominally performed but some small water leakages appeared in the lateral cooling sections of the nozzle. This phenomenon was not detected in real time as the measurements still satisfied the larger redlines margins. Figure 6 and Figure 7 respectively show the behaviour of the water cooling for the chamber and the nozzle section. Some fluctuations on the outlet pressure signal of the nozzle can be observed while the behaviour on the chamber section is nominal.

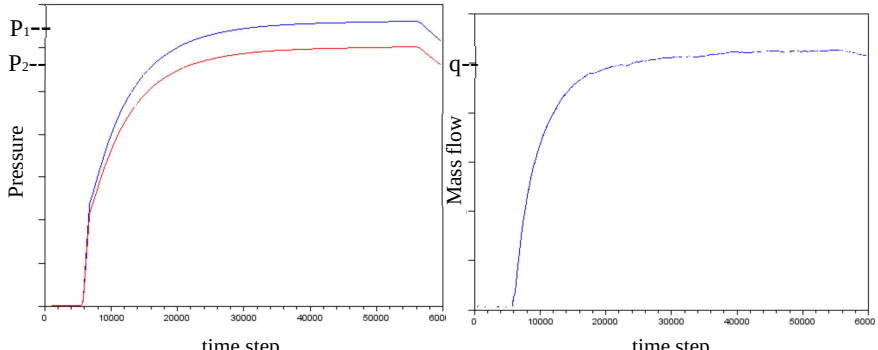

Figure 6. Chamber section V2: pressure signals, blue = inlet and red = outlet pressures, mass flow on the right

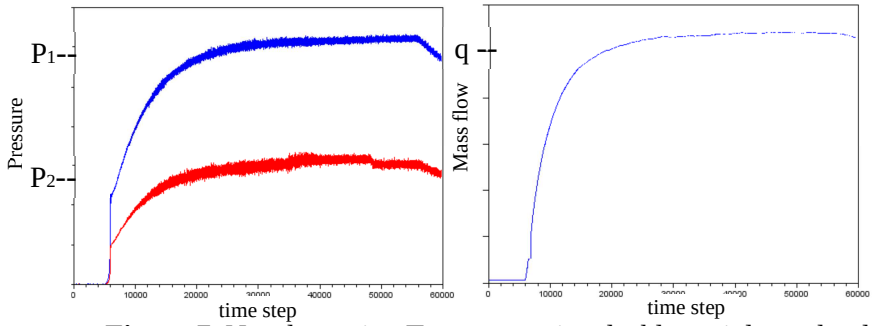

Figure 7. Nozzle section T: pressure signals, blue = inlet and red = outlet pressures, mass flow on the right

9.1.1 Parameter identification

The estimated value in steady state for the parameter *c* is 0.0042 for the chamber part and 0.0018 for the nozzle part. This result is close to the expected values of Section 5 and confirms the nominal behaviour of the system. On the nozzle parameter we can also identify a small fluctuation between 30000 and 50000 time steps.This oscillation is about 1% of the nominal parameter value *c*.

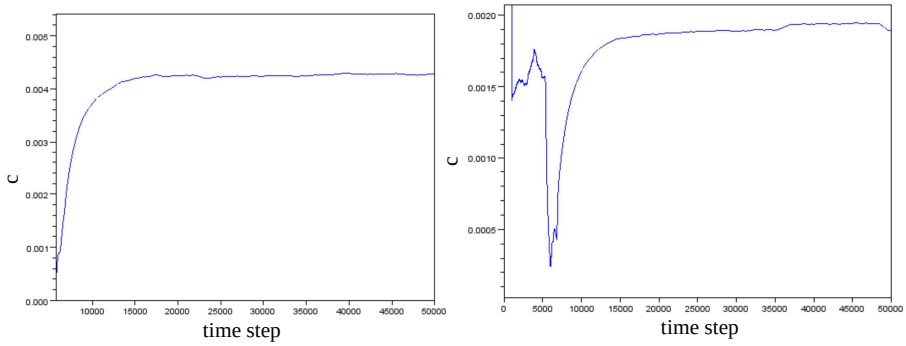

Figure 8. Estimated parameter 'c' for chamber (left) and nozzle (right)

The CUSUM test is set with δ=0.5% of *c* (that is 0.00001) and a threshold $\lambda = 3\delta$. The CUSUM and the detection flag for the nozzle part is shown below.No detection flag is raised for the chamber part, which allows isolation of the small fault on the nozzle.

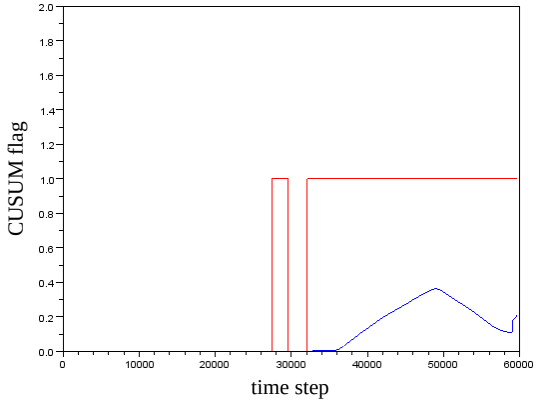

Figure 9. Nozzle CUSUM parameter (blue) and detection flag (red), δ =0.5% of *c*, λ= 3δ

Some other fluctuations are detected at around 25000 time steps but these cannot directly be associated to the pressure fluctuations. With less stringent CUSUM parameter such as δ=1% of *c* (δ=0.00002) and thresold λ=5δ it is possible to tune the test on the desired oscillations only.

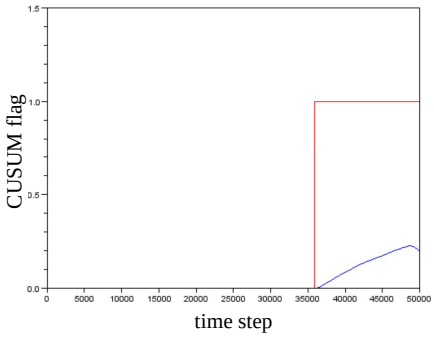

Figure 10. CUSUM parameter (blue) and detection flag (red), δ= 1% of *c*, λ=5*δ*

The small variations of system variables, as those linked to the small water leakages, are visible on the identified parameter *c* but it is not possible to discriminate which variable produced them. The CUSUM test allows to raise a detection flag when the parameter has fluctuations and it needs to be tuned to the *c* parameter fluctuations, not those of the variables.

9.1.2 Kalman filter

The Kalman filter is able to follow very efficiently the pressure signal. The residual at each step is negligible.

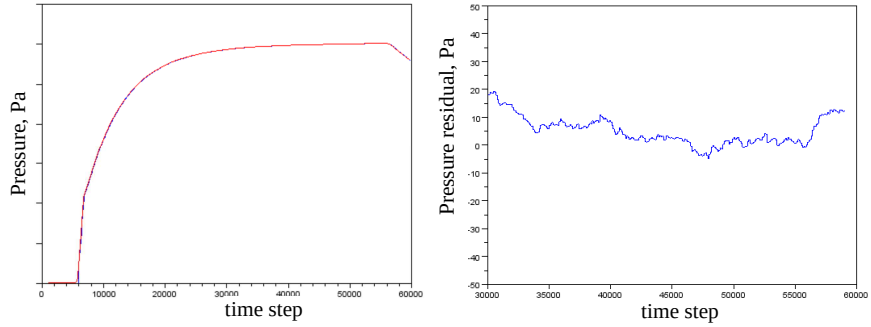

Figure 11. The estimated pressure signal (outlet) for the outlet of the chamber section and the measurement overlap (image on the left). The residual for the selected time frame of the faults (right) is negligible less than 0.1 % of the value.

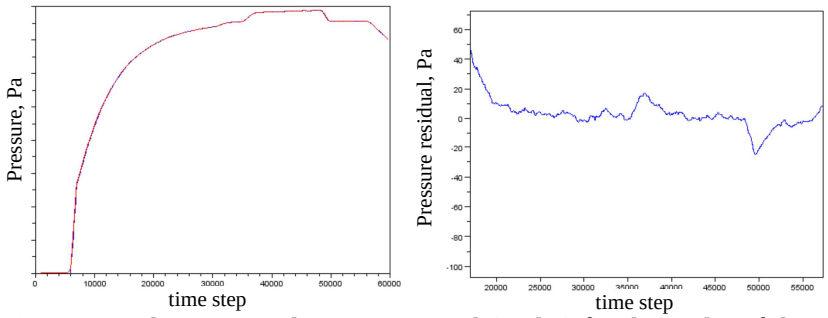

Figure 12. The estimated pressure signal (outlet) for the outlet of the nozzle section and the real measurement overlaps (image on the left). On the right is the residual for the selected time frame of the faults.

The residual curve for the nozzle part (Figure 12) shows two small variations at the time of the pressure measurement fluctuations: they correspond to the Kalman correction to follow the new trend of the pressure. The CUSUM test for the nozzle part is run during the steady state with δ=10 corresponding to the order of magnitude of the residual in the steady state nominal operation and the

maximum allowed threshold is set to $\lambda = 3\delta$. A flag is raised during the transient phase of the fluctuations: when the pressure slightly increases and when it slightly decreases to set to its expected nominal value.

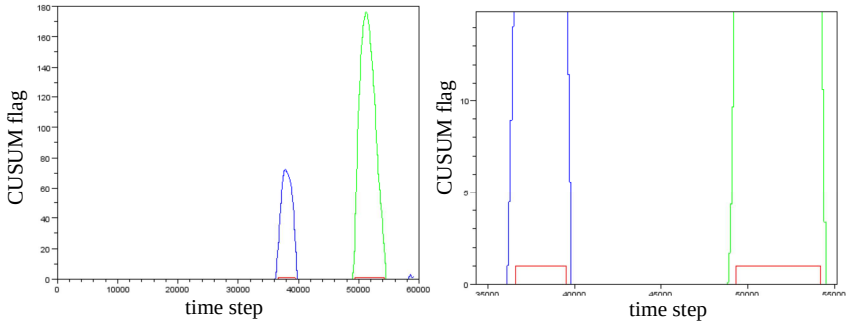

Figure 13. CUSUM flag for the outlet pressure measurement for the overall firing time frame on the left, and zoom for the time frame of the pressure fluctuations.

10 Synthesis of results and comparison with redlines

The aim of this work was to build up a set of tools to enhance currently used monitoring techniques for rocket engine and associated demonstrators. The results obtained so far showed multiple aspects for future developments:

- the parameter identification method coupled with the simplified model has been validated on the real data as the expected numerical values for the estimated parameter *c* has been obtained for the chamber and nozzle section during different test run;
- the Kalman filter approach allowed to produce a good estimate of the pressure measurements;
- the two algorithms are very simple to use and they are generic and applicable without modifications for different test run with different operating points;
- the CUSUM test provides a good tool for detection; it may require tuning on non-physical algorithm parameters such as *c* in case of parameter identification, or it may be based on the Kalman innovation variance. Via the CUSUM it was possible to detect small faults either on the identified parameter *c* or on the Kalman estimate of the pressure. The main difference in the two approaches is that in case of detection with the *c* parameter the fault cannot be associated to one measurement.

Some advantages of these technics compared to the classical redlines are the following:

- Parameter identification approach:
  - only one redline on parameter *c* is needed, compared to the three redlines for inlet/outlet pressures and mass flow monitoring,
  - the estimated parameter and its threshold do not depend on the operating point but only on geometrical data of the system and are always the same for different test runs. This is an important advantage over redlines which have to be set for each test run and can lead to human errors and unjustified tests stops.
- Kalman filtering approach:
  - the filter allows to estimate one or multiple variables and allows to detect unwanted changes;
  - coupled with the CUSUM test it can help detecting small variations into a measurement;
  - it can be used to validate a measurement.

11 Conclusions

This work is a first step towards an automatic diagnosis system for the MASCOTTE rocket engine demonstrator: the first step is to set up efficient alternatives to redlines for detection and diagnosis. This work will be completed with the improvement of the water circuit model, the analysis of other

statistical tests for detection and with the application of the algorithms to other branches of the MASCOTTE test bench.

References

[1] S.X. Ding, „Model-based fault diagnosis techniques“, Springer Verlag, Berlin Heidelberg, 2008
[2] M. Blanke, M. Kinnaert, J. Lunze, M. Staroswiecki, „Diagnosis and Fault-Tolerant Control“, Springer Verlag, Berlin Heidelberg, 2003
[3] V. Venkatasubramanian, R. Rengaswamy, K. Yin, S.N. Kavuri,”A review of process fault detection and diagnosis: Part I: Quantitative model-based methods”. Computers & chemical engineering, 27(3), 293-311, 2003
[4] R. Isermann,”Process fault detection based on modeling and estimation methods—a survey”. Automatica, 20(4), 387-404, 1984
[5] E. Chow, A.S. Willsky,”Analytical redundancy and the design of robust failure detection systems”. IEEE Transactions on Automatic Control, 29(7), 603-614, 1984
[6] J. Marzat, E. Walter, H. Piet-Lahanier, F. Damongeot, “Automatic tuning via kriging-based optimization of methods for fault detection and isolation”, 2010 Conference on control and fault tolerant systems, Nice, France, October 6-8 2010
[7] A. Iannetti, “Overview on European efforts on health monitoring/management systems for rocket engines”, Space Propulsion Conference, Köln, Germany, 2014
[8] S. Benoit, P.Bonert, S. Legonidec, P. Supié, „A diagnostic demonstrator: a platform for the evaluation of real time diagnostic data dedicated to space engines“, MFPT 2009
[9] H. Cicanek, “Space Shuttle main engine failure detection”, American control conference, Boston MA, June 19-21 1985
[10] J. Wu, “Liquid propellant rocket engines health monitoring- a survey”, ACTA Astronautica 56 (2005) 347-356
[11] IAEA Nuclear Energy Series, “On line Monitoring for improving Performance of Nuclear power plants, Part 2: Process and component condition monitoring and diagnostics”, No. NP-T-1.2, 2013
[12] G. Ordonneau, P. Hervat, L. Vingert, S. Petitot, B. Pouffary, “First results of heat transfer measurements in a new water-cooled combustor on the Mascotte facility”, 4th European conference for aerospace sciences (EUCASS), 2013
[13] I.E. Idel’cik,”Mémento des pertes de charge",3rd edition, éditions Eyrolles, 1986
[14] M. Basseville and I. Nikiforov, “Detection of abrupt changes: theory and application”, Prentice Hall, Englewood Cliffs NJ, 1993
[15] J. Marzat, H. Piet-Lahanier, F. Damongeot, E. Walter, “Model based fault diagnosis for aerospace systems: a survey”, Proceedings of the Institution of Mechanical Engineers, Part G: Journal of aerospace engineering, 226(10), 1329-1360, 2012
[16] R. Mehra, C. Rago, S. Seereeram, “Autonomous failure detection, identification and fault tolerant estimation with aerospace applications”, IEEE Aerospace Conference, 2, 33-138, 1998
[17] C. Meyer, J. Zakrajsek, “Rocket engine failure detection using system identification techniques”, AIAA-90-1993
[18] E. Cliquet, A. Iannetti, J. Masse, “Carmen, liquid propulsion systems simulation platform”, EUCASS 2009